Radio Science, Volume 20, Number 6, Pages 1452–1460, November–December 1985

High-resolution MST observations of turbulence by using the MU radar

Toru Sato, Toshitaka Tsuda, and Susumu Kato

Radio Atmospheric Science Center, Kyoto University, Uji, Japan

Shigeki Morimoto, Shoichiro Fukao, and Iwane Kimura

Department of Electrical Engineering, Kyoto University, Japan

(Received February 12, 1985; revised June 10, 1985; accepted June 26, 1985.)

The full MU (middle and upper atmosphere) radar system has been in operation since late 1984. Among various possible observations, the standard tropospheric, stratospheric, and mesospheric observations have been carried out so far. Preliminary results of turbulence observations are presented. These observations demonstrate the capability of this system and also reveal some basic scattering properties.

1. INTRODUCTION

The final stage of the construction of the middle and upper atmosphere (MU) radar at Shigaraki, Shiga, Japan (34°51'N, 136°06'E) was completed recently, and the system started its operation with all 475 yagis and 1 MW peak power in late 1984. After limited observations of the troposphere with a 57-yagi system [*Kato et al.*, 1984] for 1 year, the second stage system with 361 yagis got into operation in early 1984, which enabled lower stratospheric and mesospheric observations.

Here we present some preliminary results of upper tropospheric, lower stratospheric, and mesospheric observations, using the second stage and the final system in order to examine the basic capabilities of the MU radar such as the high height and time resolutions and the fast beam steerability. The nature of turbulence scattering at these heights is discussed.

2. SYSTEM AND OBSERVATION

The MU radar is a monostatic pulse radar operating at 46.5 MHz with an active phased array antenna system. Four hundred seventy-five yagi antennas are driven individually by solid state amplifier modules, and a peak output power of 1 MW is synthesized in space. Details of the system are described by *Kato et al.* [1984] and *Fukao et al.* [this issue].

Standard operations for MST observations utilize multiantenna beams steered every interpulse period (IPP) which enable the observer to measure line-of-sight velocities in different directions almost simultaneously. Echo power spectra at each height and beam direction are computed by the on-line array processor at the real time.

A real time fitting program is installed on the host computer VAX/11-750, which derives the echo power, Doppler velocity, and spectral width by using a nonlinear least squares fitting procedure. This procedure gives the spectral parameters with higher accuracies than the conventional spectral moment method, which tends to be affected by statistical fluctuations of the background noise component [*Sato and Woodman*, 1982*a*]. This on-line data processing program also greatly reduces the labor of the off-line processing.

The troposphere-stratosphere data presented here were taken during one 18-hour run on June 1–2, 1984, and one 24-hour run on January 6, 1985. The pulse scheme used was a 16-element complementary code with a 1-μs subpulse. The IPP was 400 μs. The antenna beam was switched every IPP and pointed in four directions in the June observation and in three directions in the January observation: vertical, north, east, and west. The zenith angle of the off-vertical beams was fixed at 15° in the June observation and at 10° in the January observation. In each

Paper number 5S0529.
0048-6604/85/005S-0529$08.00

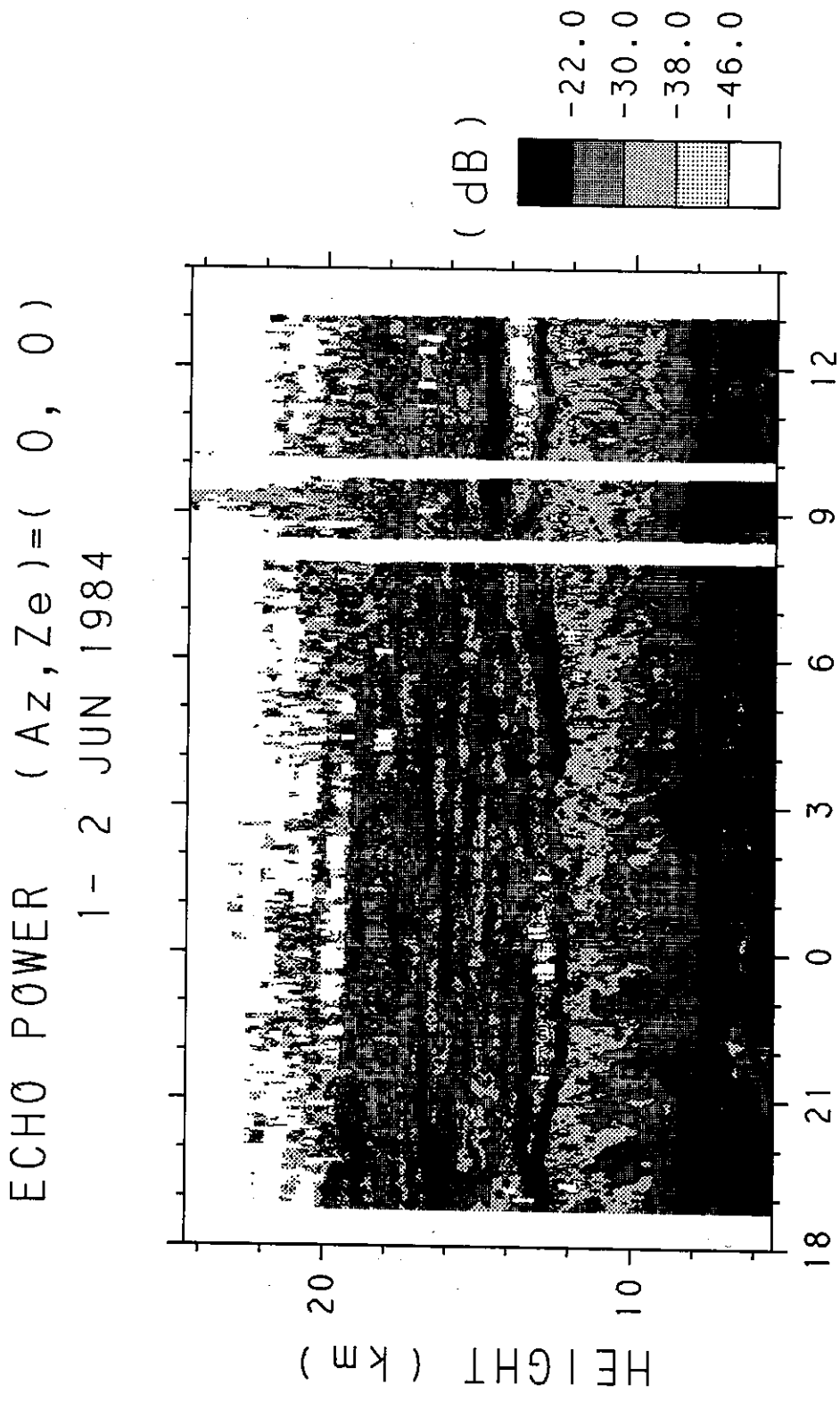

Fig. 1. Time-height contour of the echo power in the vertical direction for June 1–2, 1984. The echo power is in an arbitrary unit, and contours are drawn at 8-dB intervals.

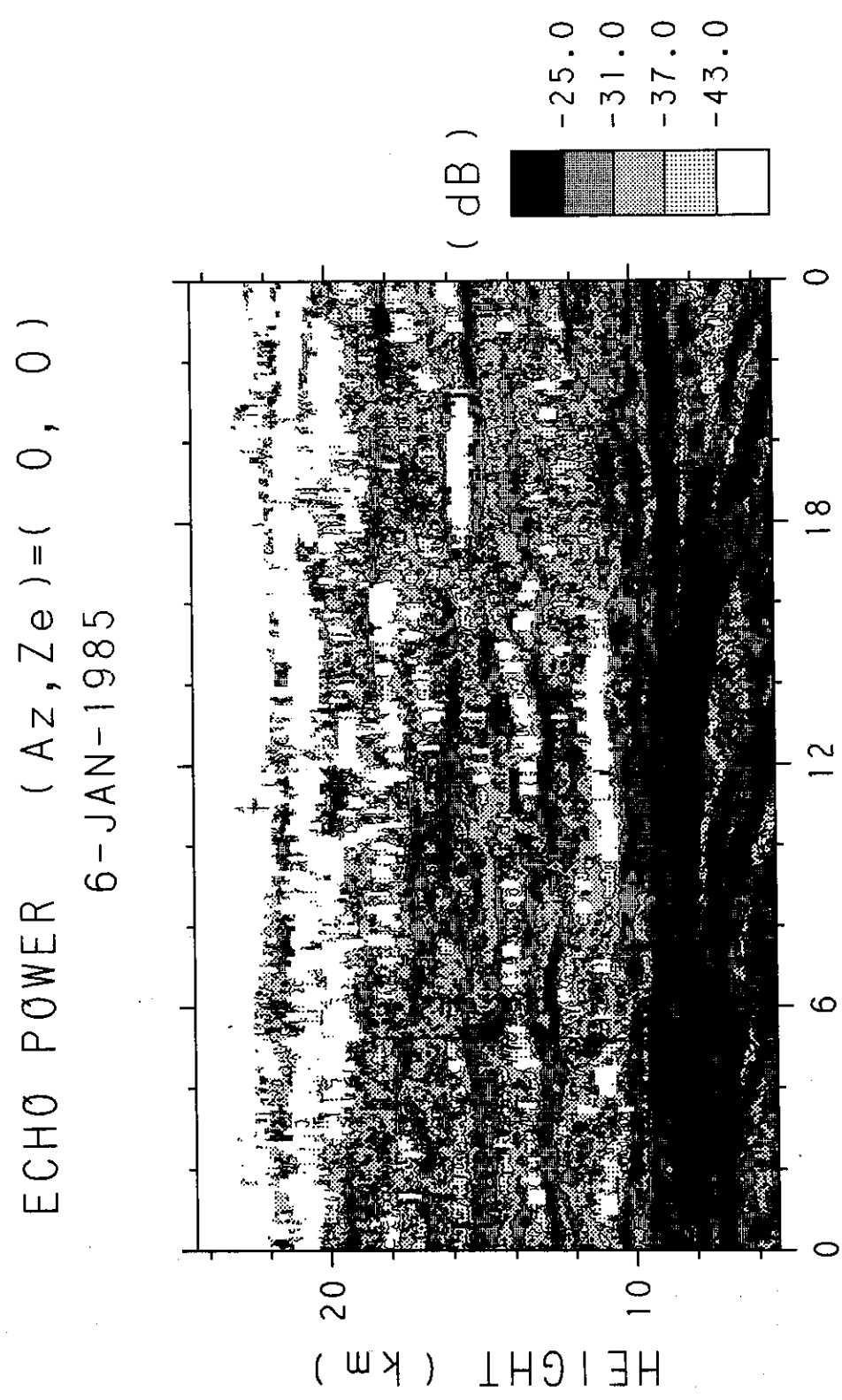

Fig. 2. Same as Figure 1 but for January 7, 1985, and at 6-dB intervals.

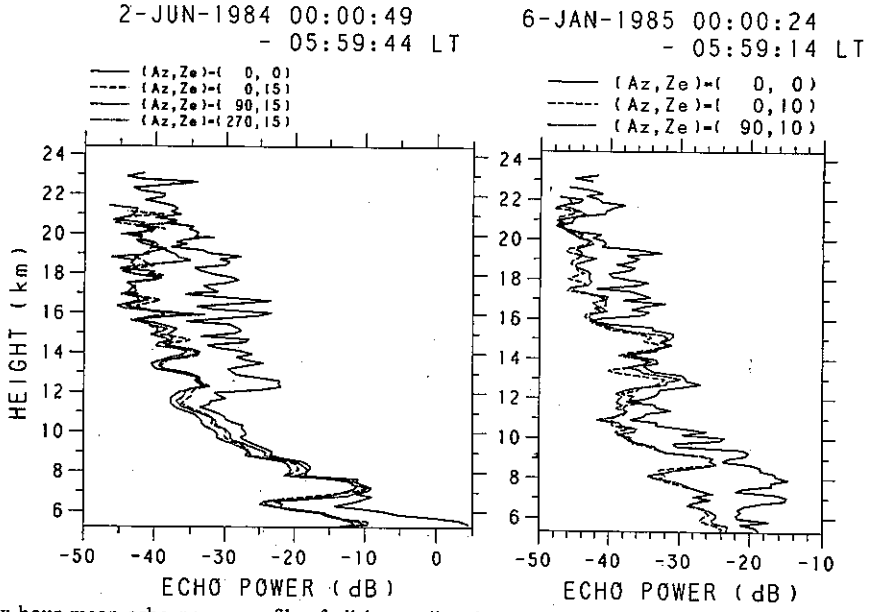

Fig. 3. Six-hour mean echo power profile of all beam directions for the (left) June and (right) January observations. Azimuth angle is measured clockwise from the north, i.e., 90° is to the east. No range correction is made.

direction, 128 heights in the range 5.4–24.5 km were sampled at 150-m intervals. Echo power spectra were computed at each height by using a 128-point FFT algorithm. The data were averaged over 1 min before recording on the magnetic tapes.

The mesospheric data shown below were taken during the 28-hour run on June 20–22, 1984, using the second stage system of 361 yagis with 760-kW peak power. The pulse scheme and beam directions were the same as those of the January observation except that the subpulse width was 4 μs, resulting in a height resolution of 600 m. The IPP was 1.3 ms and 128 heights were sampled in the 60.0- to 136.8-km region.

3. TROPOSPHERIC AND STRATOSPHERIC RESULTS

Figures 1 and 2 show the time-height contour of the scattered echo power at the upper tropospheric and lower stratospheric heights measured in the vertical direction with a time resolution of 1 min. The shading indicates the strength of the echo power in logarithmic scale. Open areas indicate that the echo power is below the detectable threshold, which is set to be 3 times the amplitude of the statistical fluctuations of the noise component.

Basic features of the scattered echo from turbulent layers are common with those found by other high-resolution VHF/UHF radars [*Röttger and Schmidt*, 1979; *Woodman et al.*, 1980; *Sato and Woodman*, 1982*b*]: strong scattering layers of 1- to 2-km thickness exhibit large time-height variability in the troposphere, often showing clear downward motion. On the other hand, separated layers in the stratosphere are much thinner and more stable. Their thickness seems to be comparable to, or even smaller than, the height resolution of 150 m.

Besides these known features, the tropospheric echo in Figures 1 and 2 shows a clear difference. A strong, diffuse layer accompanied by steeply descending patterns above is very slowly sweeping down in Figure 1, which is typical of the summer condition. On the other hand, somewhat weaker and more layered structure characterizes winter troposphere, which is in general more stable than the humid summer troposphere.

This seasonal difference is also evident in Figure 3, which compares the mean echo power profile in different antenna beam directions. Although the echo power from the troposphere largely depends on the weather conditions, such as the presence and the type of clouds and precipitations, it is more than 10 dB stronger and associates a much steeper gradient in the June data than in the January data.

The profiles in Figure 3 show clear aspect sensitivity of the scattered echo power. The aspect sensitivity

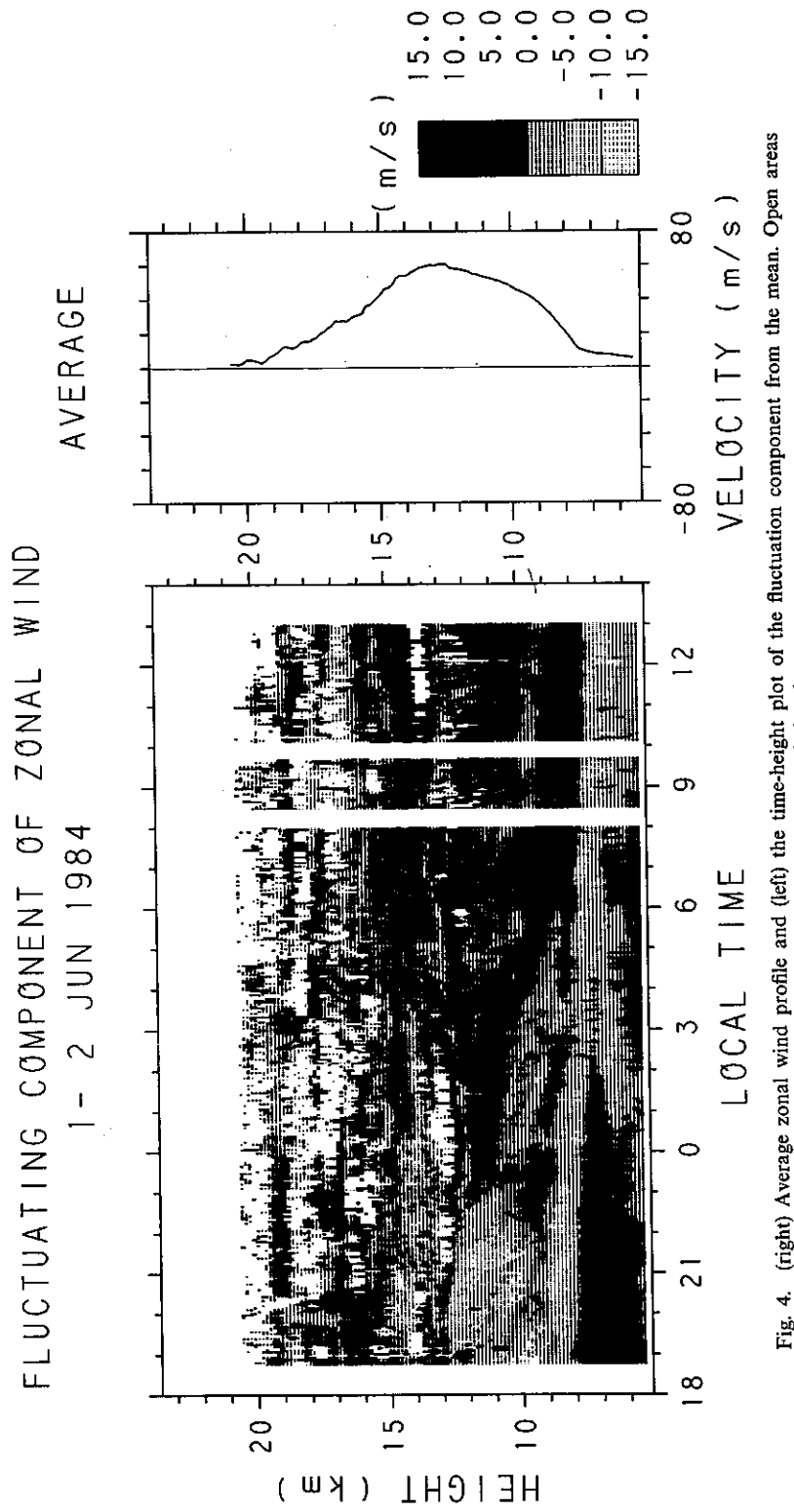

Fig. 4. (right) Average zonal wind profile and (left) the time-height plot of the fluctuation component from the mean. Open areas denote missing data.

is an indication of the inhomogeneity of the structure of scatterers at the scale size of half the radar wavelength. The most commonly used explanation for the stronger echo power in the vertical direction than in the off-vertical direction is that the radio waves are scattered by thin laminae of turbulence, or at least by turbulent layers which have sharp boundaries of the order of the radar wavelength. Large aspect sensitivity is not observed at most of tropospheric heights in the June data, while it is evident throughout the troposphere in the January data. This tendency is consistent with the more layered appearance of the echo power contour in the January data than in the June data. It is interesting that the scattering layers of the winter troposphere show characteristics quite similar to the stratospheric layers in their macroscopic appearance as well as in this aspect sensitivity, which concerns a microscopic structure at 3-m scale size.

The general tendency that stronger aspect sensitivity associates thinner and more stable layer supports the explanation of the aspect sensitivity assuming the partial reflection mechanism [*Gage and Green*, 1978].

A clear correspondence exists between the behavior of the scattering layers and the fluctuation pattern of the wind field. Figure 4 shows (right) the average zonal wind profile for the June data and (left) the fluctuation of the zonal wind around the average. The horizontal wind velocity is determined from the line-of-sight velocities in the vertical and eastward directions of the same 1-min data, assuming spatial homogeneity of the wind field. This assumption introduces some error if there exists a wave with a short horizontal wavelength and a large vertical motion, which are characteristic of short-period gravity waves.

A typical observed amplitude of 1 m/s for these waves causes the maximum error of 4 m/s to the inferred horizontal velocity when the associated horizontal wavelength is 4 times the spatial separation of the scattering volumes illuminated by the two beams. The error becomes smaller for longer time scales for which the horizontal wavelength of gravity waves becomes longer. Fluctuation of the meridional component, which is not presented here, also shows a quite similar pattern to that in Figure 4.

The correspondence between turbulent layers and fluctuations in the wind field can partly be explained, especially in the stratosphere, by the generation of the turbulence due to the shear instabilities [*Sato and Woodman*, 1982*b*].

Figure 5 shows the total vertical shear of horizontal winds averaged over the entire period shown in Figure 4, and the Richardson number profile derived from this shear profile and the temperature data obtained by two rawinsondes launched at Shionomisaki (150 km south to the radar site) during this period. The average Richardson number profile indicates that most of the 7- to 18-km region is always in, or close to, the subcritical state, which is defined by the Richardson number of 0.25–1.0, if the fact is taken into account that the height resolution of 150 m is not good enough to resolve local shear structures.

Instantaneous values of the Richardson number, obtained by assuming that the temperature profile is stable over the observed period, often become quite small and sometimes reach 0.25. The fact that it always takes positive value seems to suggest that the shear instability plays a major role, although the possibility of the convective instability cannot be ruled out because of sparse data points in the temperature data.

Other mechanisms such as the enhancement of echoes due to the presence of water vapor or strong convection inside clouds may contribute to the relation between the echo power and the wind velocity fluctuation in the troposphere.

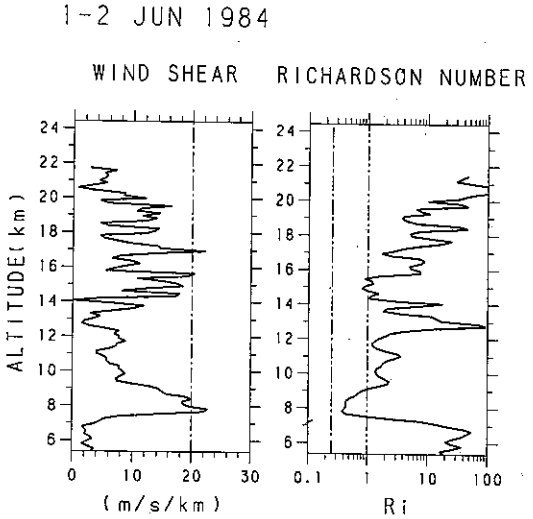

Fig. 5. Average profiles of the vertical shear of horizontal winds (left) and the Richardson number for the whole period of Figure 4.

4. MESOSPHERIC RESULTS

Fine altitude resolution observations using VHF radars have revealed stratified structures of the tur-

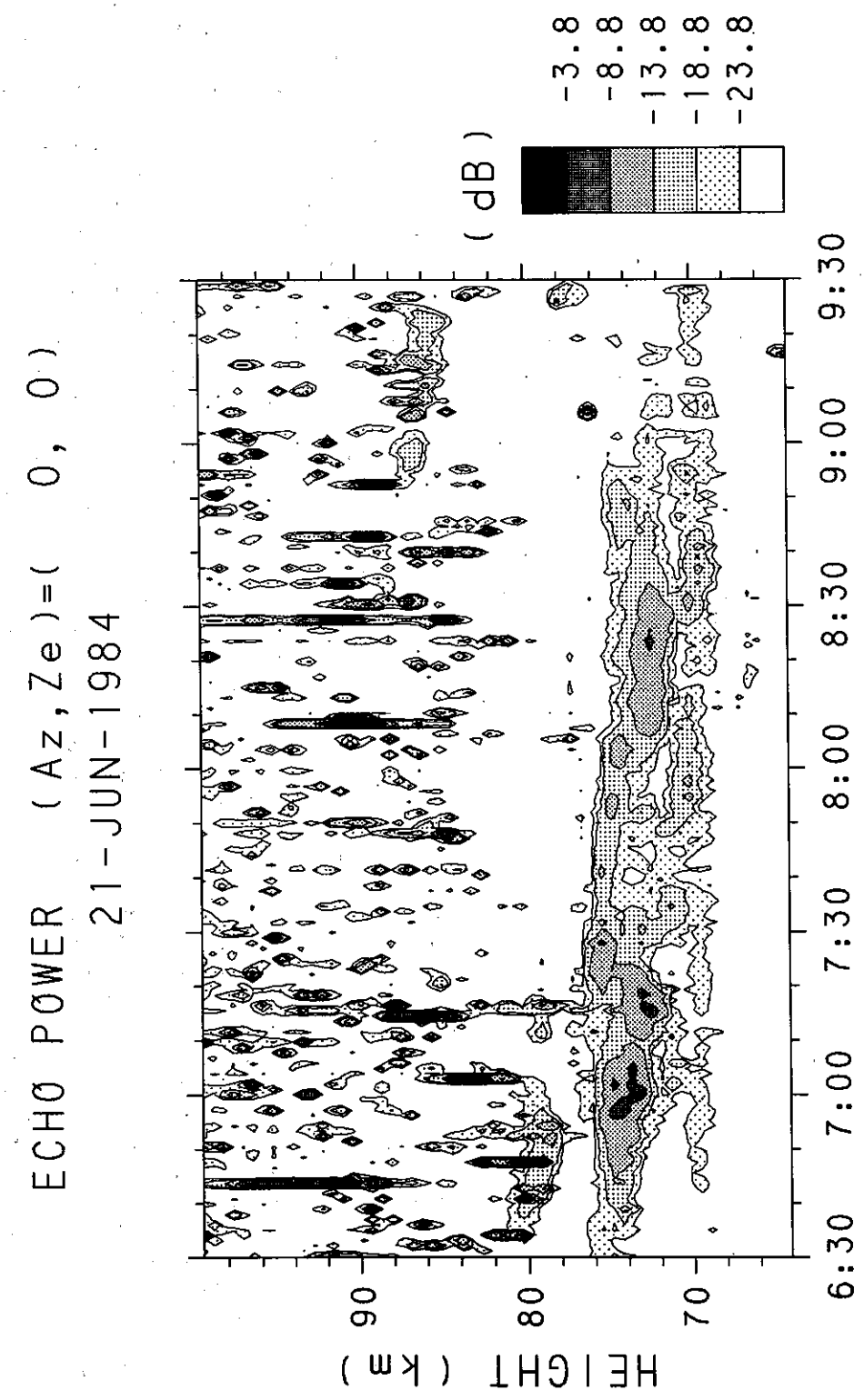

Fig. 6. Time-height contour of the mesospheric echo power in the vertical beam direction.

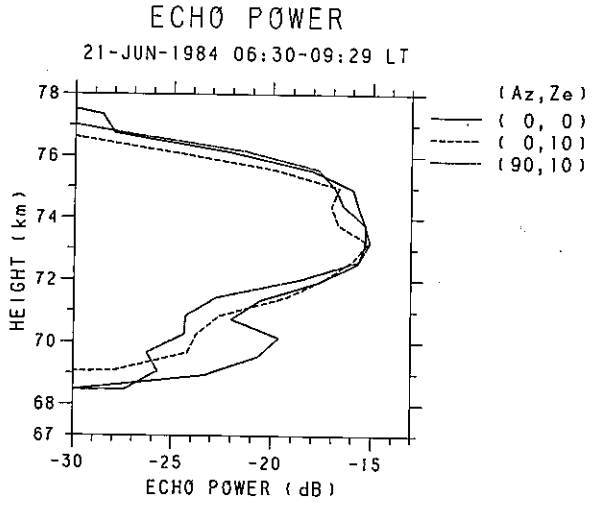

Fig. 7. Average echo power profile of the three beam directions for the period of Figure 5.

bulence scattering from the mesosphere [*Czechowsky et al.*, 1979; *Röttger et al.*, 1981]. The fast beam steerability of the MU radar adds the ability to study spatial and angular dependence of the scattering to those observations without losing the high sensitivity.

Figure 6 shows a time-hieght contour of the mesospheric echo power in the vertical direction when a fairly strong turbulence echo is observed in the 70- to 75-km region. The time resolution is 1 min. There seem to be two different kinds of turbulent layers in this height range. One is the layer at 70 km, which is fairly stable in height, and the other is the stronger layer around 74 km, which shows repetition of descending motion. These two layers, although close to each other, have different aspect sensitivity, as shown in Figure 7. This figure depicts the average echo power in three antenna beam directions versus height for the whole period of Figure 6. The vertical echo power is about 5 dB stronger than that in the other two directions for the layer at 70 km, while no clear aspect sensitivity can be seen for the echo at 72–76 km except for a slight difference at 75 km.

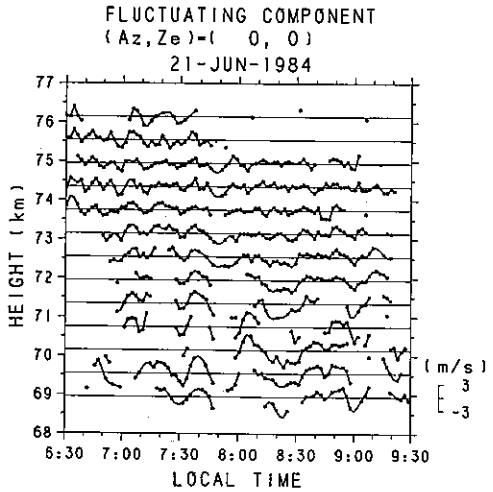

Fig. 8. Vertical wind velocity around the temporal mean at each height. Each dot stands for a 2-min mean echo power. Lines are not connected when there are three or more missing data between two dots.

Although previously found by other VHF radars [*Fukao et al.*, 1979; *Röttger et al.*, 1979], this aspect sensitivity in the mesospheric echo has not yet been studied in detail due to the lack of altitude resolution and sensitivity. The present data provide a better image of the mesospheric turbulent layers, in that they reveal a clear relation between the aspect sensitivity and the mesospheric layer thickness and stability, which turned out to be quite similar to that found in the stratosphere.

However, the aspect sensitivity in the mesospheric echo requires a different mechanism from the stratospheric one, because the strict partial reflection condition cannot be satisfied at this height where the minimum scale of turbulence exceeds the radar wavelength [*Röttger et al.*, 1979]. This resemblance of the stratospheric and mesospheric scattering morphology seems to support the explanation that the weak (or diffuse) Fresnel reflection is contributing to the mesospheric echoes in addition to the isotropic turbulence scattering.

The mechanism which contributes to the different nature between the two layers in Figure 6 is not clear from our limited data. However, if we consider that the mesospheric echo power is determined by the product of the electron density gradient and the strength of turbulence, the layer at 70 km would associate a stronger turbulence than the layer at 72–76 km because the electron density and its gradient is increasing drastically with height in this region. If so, localized strong shear may contribute to the aspect-sensitive layer at 70 km.

No direct correspondence is found between the shape and motion of the scattering layers and the wind fluctuation as observed in the stratosphere. Figure 8 shows the fluctuating component of the vertical wind velocity versus time at each height at 2-min intervals. Although it is rather hard to carry out a spectral analysis due to the lack of data, the typical period of fluctuation tends to decrease with

height as found by *Fukao et al.* [1979] at Jicamarca, Peru. Rapid oscillations around 75-km height have a period of less than 10 min, close to the Brunt-Väisälä period at this height range.

5. CONCLUSIONS

Characteristics of the tropospheric, stratospheric, and mesospheric turbulence scattering observed by the MU radar have been presented and discussed. The fine time and height resolution of 1 min and 150 m, respectively, of the MU radar, along with the fast beam steerability, made it possible to study the nature of the atmospheric turbulent layers both from their macroscopic appearance as well as the microscopic feature characterized by the aspect sensitivity of the echo power.

Two data sets of the tropospheric and stratospheric observations representing the summer and winter seasons showed an example of seasonal variability of the tropospheric scattering. The strong shear which associates thin turbulent layers in the stratosphere supports the argument for the generation of turbulence by the shear instability mechanism.

A standard feature is found in the morphology of the turbulence that strong aspect sensitivity associates with stable layer structures throughout the troposphere, stratosphere, and mesosphere, despite the possible difference in the mechanism which causes the aspect sensitivity in the stratosphere and mesosphere.

Acknowledgments. The authors wish to thank M. Inaba of the Department of Electrical Engineering, Kyoto University, for his help in the data analysis. Part of the data analysis was performed at the Data Processing Center of Kyoto University.

REFERENCES

Czechowsky, P., R. Rüster, and G. Schmidt, Variations of mesospheric structures at different seasons, *Geophys. Res. Lett.*, *6*, 459–462, 1979.

Fukao, S., T. Sato, S. Kato, R. M. Harper, R. F. Woodman, and W. E. Gordon, Mesospheric winds and waves over Jicamarca on May 23–24, 1974, *J. Geophys. Res.*, *84*, 4379–4386, 1979.

Fukao, S., T. Sato, T. Tsuda, K. Wakasugi, S. Kato, and T. Makihira, The MU radar with an active phased array system, *Radio Sci.*, this issue.

Gage, K. S., and J. L. Green, Evidence for specular reflection from monostatic VHF radar observations of the stratosphere, *Radio Sci.*, *13*, 991–1001, 1978.

Kato, S., T. Ogawa, T. Tsuda, T. Sato, I. Kimura, and S. Fukao, The middle and upper atmosphere radar: First results using a partial system, *Radio Sci.*, *19*, 1475–1484, 1984.

Röttger, J., and G. Schmidt, High resolution VHF radar soundings of the troposphere and stratosphere, *IEEE Trans. Geosci. Electron.*, *GE-17*, 182–189, 1979.

Röttger, J., P. K. Rastogi, and R. F. Woodman, High-resolution VHF radar observations of turbulent structures in the mesosphere, *Geophys. Res. Lett.*, *6*, 617–620, 1979.

Röttger, J., P. Czechowsky, and G. Schmidt, First low-power VHF radar observations of tropospheric, stratospheric and mesospheric winds and turbulence at the Arecibo Observatory, *J. Atmos. Terr. Phys.*, *43*, 789–800, 1981.

Sato, T., and R. F. Woodman, Spectral parameter estimation of CAT radar echoes in the presence of fading clutter, *Radio Sci.*, *17*, 817–826, 1982*a*.

Sato, T., and R. F. Woodman, Fine altitude resolution observations of stratospheric turbulent layers by the Arecibo 430 MHz radar, *J. Atmos. Sci.*, *39*, 2546–2552, 1982*b*.

Woodman, R. F., R. P. Kugel, and J. Röttger, A coherent integrator-decoder preprocessor for the SOUSY-VHF-radar, *Radio Sci.*, *15*, 233–242, 1980.

S. Fukao, I. Kimura, and S. Morimoto, Department of Electrical Engineering, Kyoto University, Kyoto 606, Japan.

S. Kato, T. Sato, and T. Tsuda, Radio Atmospheric Science Center, Kyoto University, Uji 611, Japan.